Journal of the Ceramic Society of Japan 128 [10] 783-789 2020
DOI http://doi.org/10.2109/jcersj2.20126

JCS-Japan

FULL PAPER

Low-temperature mineralization sintering process of bioactive glass nanoparticles

Yeongjun SEO[1], Tomoyo GOTO[1], Hisataka NISHIDA[1], Sung Hun CHO[1], Aleksej ZARKOV[2], Taisei YAMAMOTO[1] and Tohru SEKINO[1,†]

[1]The Institute of Scientific and Industrial Research, Osaka University, 8–1 Mihogaoka, Ibaraki, Osaka 567–0047, Japan
[2]Institute of Chemistry, Faculty of Chemistry and Geosciences, Vilnius University, Naugarduko 24, Vilnius, LT-03225, Lithuania

Inspired by biomineralization in nature which provides the formation of various inorganic minerals under mild temperatures and pressures conditions, we report here the low-temperature mineralization sintering process (LMSP) of SiO_2–CaO–P_2O_5 bioactive glass nanoparticles (BGNs). The ternary BGNs were successfully synthesized by an alkali mediated sol–gel method. The obtained glass nanoparticles, having around 30 nm in diameter, were sintered in a mold under an applied pressure of 300 MPa at 120 °C with an aid of small amount of simulated body fluid (SBF) solution. Under the condition, BGNs were densified through biomineralization with a formation of amorphous calcium phosphate phase which filled up the interparticle boundaries and bonded each glass nanoparticles. The relative density and Vickers hardness of the sintered BGNs were sufficiently high, 86 % and 2.09 GPa, respectively, although the low sintering temperature. These values were higher than those of BGNs sintered by the same procedure with no aqueous solution (57 %, 0.68 GPa), distilled water (77 %, 1.52 GPa), and even the conventionally sintered BGNs at 550 °C (69 %, 0.93 GPa) and 850 °C (81 %, 2.02 GPa). These results suggest that the LMSP is a promising and cost-effective process for obtaining bioactive glass and ceramic bulk materials at low temperature.

Key-words : Low-temperature sintering, Biomineralization, Bioactive glass, Simulated body fluid, Calcium phosphate

[Received May 23, 2020; Accepted July 18, 2020]

1. Introduction

Sintering process has been widely investigated to obtain bulk materials from powders as starting materials.[1)–3)] This process is typically assisted by thermal energy and/or pressure. In the field of ceramic science, conventional solid-state sintering is generally performed at temperature higher than 1000 °C to obtain dense ceramics. With development of industrial technologies, to reduce the sintering temperatures, the sintering processes have been developed by utilizing liquid phases, pressure, or electric fields such as liquid phase sintering, hot pressure sintering, and field-assisted sintering technique.[4)–6)] In contrast, hard tissue in living organisms is formed under ambient temperature and pressure conditions. This process is called biomineralization that provides various inorganic-based structures such as carbonates and phosphates (including corals, shells, and bones),[7)] and many researches have been aggressively carried out and reported. In the case of bone, bone mineral is formed on collagen fibers by the action of cells such as osteoblasts using Ca^{2+} and PO_4^{3-} ions in body fluids.[8)] The challenge of implementing the natural process like the biomineralization in the sintering technology makes it possible to achieve technological innovation for great energy savings and cost reduction. For this purpose, the materials, which can induce the biomineralization, are required; for example, biomaterials such as bioactive glasses (BG) are known to show the apatite-forming ability through the mechanism of biomineralization in human body without cells.[9)]

BG are generally SiO_2-based glasses, containing CaO, P_2O_5, Na_2O, and so on.[10)] In the case of SiO_2–CaO–P_2O_5 system BG, SiO_2 and P_2O_5 are network formers, and CaO is a commonly used network modifier. They have been widely used as biomaterials for human's bone and teeth due to their biomineralization. In addition, BG have been increasingly studied for coatings of inactive metal materials for load bearing applications and obtaining the stable interfacial bonding with tissues.[11),12)] In an aqueous medium such as body fluids, Ca^{2+} or PO_4^{3-} ions are released from the bioactive glass, forming Si–OH and a SiO_2 gel layer on the surfaces of the bioactive glass through the condensation and repolymerization of Si–OH. Then, amorphous calcium phosphate forms as hydroxyapatite, HAp, or bone-like apatite by consuming the Ca^{2+} and PO_4^{3-} ions.[13)] There-

† Corresponding author: T. Sekino; E-mail: sekino@sanken.osaka-u.ac.jp

fore, for the development of biomimetic sintering technologies, the process design of chemical reaction is important to reproduce the above biological reaction.

In recent developments in sintering technology, cold sintering process (CSP) was reported as a remarkably low temperature sintering technique, inspired by geological mineral formation.[14] CSP is a non-equilibrium densification process of ceramic powders at low temperatures below 300 °C under a uniaxial pressure from 100 to 500 MPa.[14),15] CSP significantly promotes densification and crystal growth of ceramic materials through mechanical-chemical kinetics using a transient phase from moistened ceramic powders, containing liquids such as water or acidic solutions. During CSP, the moistened particles are initially compacted and rearranged under external uniaxial pressure of MPa magnitude. At the same time, the aqueous solution dissolves the particles and then, the liquid components are evaporated by the controlled temperature below 300 °C. This evaporation introduces a supersaturated solution with respect to component at the surfaces of the particles. Finally, this transient supersaturated phase is precipitated and then crystal growth occurs at the final stage of CSP. Using this sintering process, Randall et al.[16)–18)] have successfully obtained various bulk ceramic materials such as $BaTiO_3$, ZnO, and over 50 species of ceramics. In addition, Bouville and Studart[19)] used CSP for densification of nano-vaterite particles at room temperature. However, despite the great possibility of the application of CSP to various inorganic materials, very few studies, related to the low-temperature consolidation of glass materials, have been reported.[20)]

Here, we propose a novel low-temperature densification route for BG, called low-temperature mineralization sintering process (LMSP). LMSP is derived from the biomineralization of BG in vivo. To reproduce the biomimetic environment, simulated body fluid (SBF), whose ion concentration and pH close to those of human blood plasma,[21)] is used in this process. Through the mechanical-chemical kinetics based on CSP, the mixture of SBF solution and bioactive glass can induce the biomineralization to form a calcium phosphate phase, leading to the densification of the BG at low temperature level. Thus, LMSP provides a dense biphasic material, which consists of bioactive glass with the calcium phosphate, unlike CSP in which a pure single phase is observed.[15)] In the present study, bioactive glass nanoparticles (BGNs) were synthesized and used to enhance the biomineralization reaction because of higher specific surface area and curvature of nanoparticles that resulted in higher Gibbs free energy at the surface. To densify the BG at low temperature, here at 120 °C, BGNs were mixed with SBF solution, and the mixture was pressed and heated concurrently under the hydrothermal conditions. The effect of biomineralization on the densification and mechanical properties of sintered BG was investigated by comparing the LMSP sample with other samples sintered by different solution conditions and conventionally sintering samples. Finally, the densification mechanism of LMSP was discussed in details.

2. Materials and methods

2.1 Synthesis of bioactive glass nanoparticles (BGNs)

The synthesis method of BGNs [SiO_2:CaO:P_2O_5 (mol %) = 55:40:5] was based on the previously reported procedure and briefly described as follows.[22)] Tetraethyl orthosilicate (TEOS), calcium nitrate tetrahydrate (CN) and ammonium dibasic phosphate (ADP) were used as precursors for SiO_2, CaO and P_2O_5, respectively, and purchased from FUJIFILM Wako Pure Chemical Corporation (Japan). First of all, TEOS-ethanol solution, created by adding 9.84 mL of TEOS into 60 mL of ethanol, was poured into 120 mL of pure water solution, containing 7.639 g of CN. Then, citric acid (FUJIFILM Wako Pure Chemical Corporation, Japan) was added into the mixture solution to adjust the pH value to 1–2. After the pH controlled solution became transparent, the solution was slowly dropped into 1500 mL of the ammoniated deionized water, containing 1.078 g of ADP. During homogenization, the pH value of final solution was kept approximately 11 using ammonia water (FUJIFILM Wako Pure Chemical Corporation, Japan) and the solution was vigorously stirring for 48 h and aging for 24 h. Finally, after the precipitate was freeze-dried and calcined at 700 °C for 3 h, white BGNs were obtained.

2.2 Low temperature densification process using biomineralization

To homogeneously induce biomineralization, 3.0 g of the obtained BGNs were mixed with 25 wt % SBF solution, prepared by Kokubo's method.[23)] Then, the moistened BGNs by SBF solution were put into the pre-heated mold at 120 °C. The mold was pressed under 300 MPa uniaxial pressure, using newton press model, at 120 °C for 10, 20, 30, and 60 min. After the pressing, the LMSP sample (hereafter denoted as BG/SBF) were washed three times with distilled water and dried in the oven overnight at 60 °C. In the other experiments, to evaluate the effect of SBF solution on biomimetic mineralization of LMSP, the BGNs were densified without any aqueous solutions (BG/dry) and with 25 wt % distilled water (BG/water) instead of SBF solution under the same pressure and heat treatment conditions. Additionally, the green body of BGNs, pressed under 160 MPa, was sintered at 550 °C (BG/550) and 850 °C (BG/850) for 2 h to observe the effect of LMSP on densification and Vickers hardness of the sintered BGNs in comparison with the conventional sintering process.

2.3 Characterization

The bulk densities were measured by Archimedes method using absolute ethanol as a liquid media, and average density values were chosen from the samples. To measure the relative density, true densities of glass nanoparticles (BGNs) and sintered samples were measured by an electronic densimeter (MDS-300, Alfa Mirage Co., Lid., Osaka, Japan) with absolute ethanol as a liquid media:

each sintered samples were carefully crashed to obtain fine powders below 0.4 μm in size, which were considered not to contain either open or closed pores. The relative density was then calculated using the true and bulk density. Fracture surfaces of each sintered sample were observed by a field-emission scanning electron microscope (FE-SEM, SU9000, Hitachi High-Tech Corp., Tokyo, Japan) at 30 kV. Before SEM observation, the samples were coated by Osmium plasma coater (OPC-60A, SPI Supplies, PA, USA) without polishing to confirm the original microstructural feature. Vickers hardness was measured using a Vickers hardness tester (FV-310e, Future-tech Corp., Kanagawa, Japan) six times for each sample under 19.8 N of an applied load and holding time of 15 s, and the average values were achieved. The structural analysis of the sintered samples was conducted by X-ray diffraction (XRD, D8 Advance, Bruker AXS GmbH, Karlsruhe, Germany) with Cu $K\alpha$ radiation. XRD patterns were collected at 40 kV and 40 mA from $2\theta = 10$ to 60° with a step size of 0.02°. X-ray Fluorescence (XRF, ZSX100e, RIGAKU Corp., Tokyo, Japan) was performed to determine compositional changes after the sintering processes. To observe chemical conversion of the sintered samples by biomineralization, Fourier transform infrared spectroscopy (FT-IR, FT/IR4100, JASCO, Tokyo, Japan) was performed.

3. Results and discussion

3.1 Density and microstructure

To compare the densification behavior of BG/SBF with that of BG/dry and BG/water and to estimate the effect of biomineralization on the densification of BGNs, BGNs were densified under exactly same conditions except using the aqueous solutions. For the comparison, the relative density of each sintered sample was introduced. However, the theoretical density of each sintered sample was different because BGNs were densified by the precipitation of calcium phosphate during LMSP, and therefore, BG/SBF and BG/water may contain BGNs as well as the precipitated phase in their grain boundaries. For this reason, the calculation of theoretical density of LMSP samples are quite difficult because rule of mixture cannot be applicable in the present case. Therefore, true density of bulk samples was measured using their milled powders. The true density of BGNs was also measured and determined to be 2.56 g/cm^3, which value was used to estimate relative density of BG/dry, BG/550 and BG/850. This value was consistent with the reported theoretical density of bioactive glass of similar composition,[24] and also in a good agreement with the theoretical density calculated from empirical equation for calculating the density of oxide glasses.[25] In the case of bulky LMSP samples, the true densities for BG/water and BG/SBF were obtained to be 2.55 and 2.58 g/cm^3, respectively, which were considered to be reasonable values to calculate their relative densities.

Most sintered samples were completely densified after sintering for 30 min (**Fig. 1**). In the case of BG/dry, the relative density was only 57 % after sintering for 30 min.

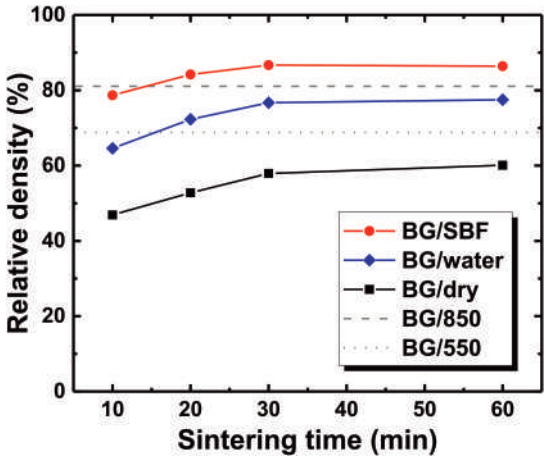

Fig. 1. Relative density of the sintered BGNs with the different conditions. The dot and dash lines refer to the relative density of BG/550 and BG/850, respectively.

On the other hand, the relative densities of BG/SBF and BG/water dramatically increased to 86 and 77 %, respectively. Densification behavior of all the sintered samples was different depending on the existence of the aqueous solutions. For BG/dry, BGNs were densified by only pressure and heat without any aqueous solutions. By contrast, during sintering of BG/SBF and BG/water, the aqueous solution played an important role in the densification of BGNs. The aqueous solution such as distilled water or SBF solution lubricates the surfaces of BGNs, and it accelerates the rearrangement of BGNs by the applying uniaxial pressure of 300 MPa at the early stage of the process, which phenomenon was already argued in the case of CSP.[14)–18)] Above all, an interesting result was that BG/SBF showed 9 % higher relative density than BG/water.

The SEM images (**Fig. 2**) of fracture surfaces also agreed with the results of density measurement. In BG/dry, there was no neck formation between BGNs while BG/water and BG/SBF showed the neck formation. However, in BG/water, there were still some pores between the coarse particles, compared with BG/dry. On the other hand, the fracture surfaces of BG/SBF showed a dense configuration with little pores in comparison with other sintered samples. We assumed that SBF solution is more effective to densify BGNs because the biomineralization was easily encouraged during densification using SBF solution instead of the distilled water. This densification mechanism will be discussed further in section 3.4.

Further, we compared densification behavior of BG/SBF with those of conventionally sintered samples at 550 °C (BG/550) and 850 °C (BG/850), respectively (**Fig. 3**). With increase in sintering temperatures from 550 to 850 °C, the relative density also increased from 69 to 81 % (Fig. 1). However, even though the relative density of conventionally sintered BGNs was improved by increasing the sintering temperature, the density of BG/SBF was still 5 % higher than that of BG/850 although the processing temperature was significantly lower. In addition, even though the neck formation of BGNs was observed in the

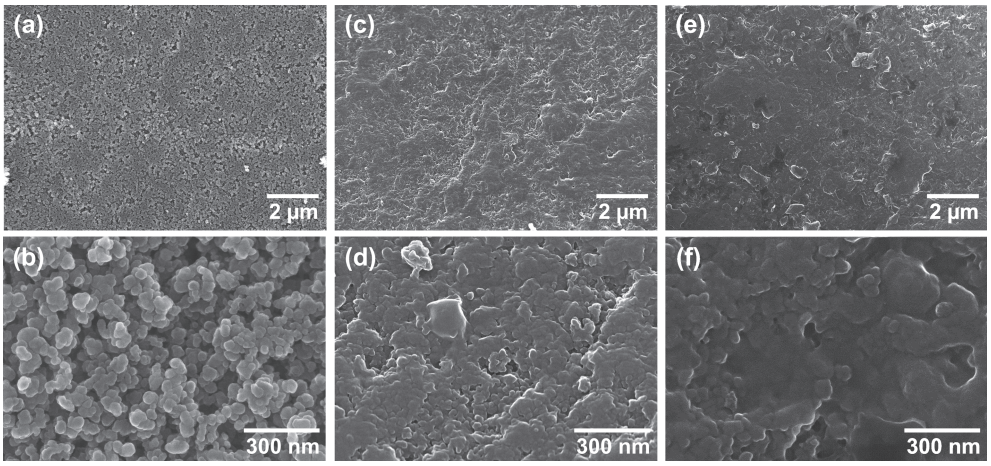

Fig. 2. Fracture surfaces of (a)–(b) BG/dry, (c)–(d) BG/water, and (e)–(f) BG/SBF.

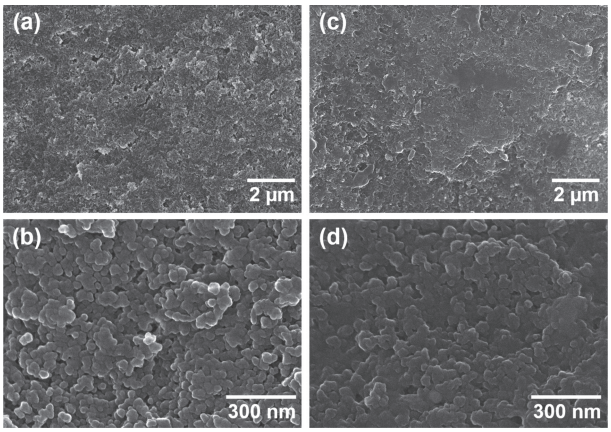

Fig. 3. Fracture surfaces of (a)–(b) BG/550 and (c)–(d) BG/850.

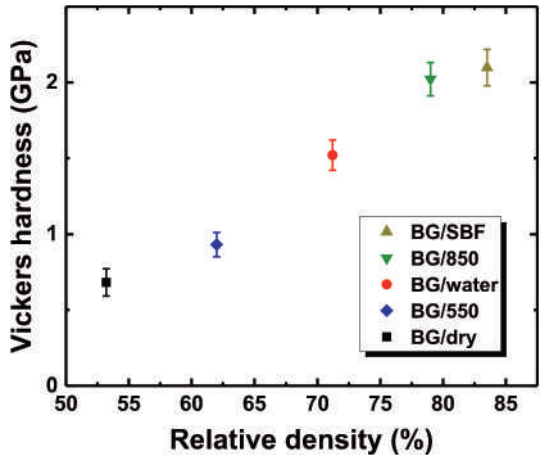

Fig. 4. Vickers hardness of the sintered BGNs under different conditions.

fracture surface of BG/850, the fracture surface of BG/SBF showed denser figuration with less pores.

3.2 Vickers hardness test

To observe the mechanical properties of the sintered samples after sintering for 30 min, Vickers hardness test was carried out. The Vickers hardness was plotted against the relative densities of the sintered samples including the conventionally sintered samples (**Fig. 4**). All the samples were analyzed without mechanical polishing. Vickers hardness of BG/SBF (2.09 GPa) was the highest among the samples sintered by the same condition such as BG/dry (0.68 GPa) and BG/water (1.52 GPa), and even higher than that of conventionally sintered samples at higher temperatures, BG/550 (0.93 GPa) and BG/850 (2.02 GPa). These are in good agreement with the results of the relative density and the microstructural features as mentioned before.

Furthermore, it was confirmed that Vickers hardness of the sintered samples increased with increasing their relative densities regardless of their sintering mechanisms. In other words, there is a relation between density and hardness in the bulky materials, which is a quite appropriate phenomenon. These results proved that LMSP can provide the sintered BGNs with mechanical properties equivalent to that of the conventionally sintered body using much lower thermal energy. From these results, we expect that the chemical environments such as existing ions and pH value of SBF solutions as well as applied pressure may enhance dissolution of further chemical species from BGNs and followed precipitation of inorganic phases, i.e. biomineralization process, and also contribute to obtain the higher relative densities and the better microstructures. In addition, the LMSP seems more efficient than the conventional sintering process.

3.3 Observation of biomineralization during LMSP

In bioactive glass materials, the biomineralization is generally carried out in SBF solution at 37 °C for several days, forming crystalline HAp.[26] However, in this study, the biomineralization would be induced at 120 °C for 10, 20, 30, and 60 min, based on the results of the improved densification and Vickers hardness. Therefore, XRD analysis was performed to characterize the phase development in accordance with the densification process (**Fig. 5**), and

the compositional changes of the sintered samples were demonstrated by XRF analysis (**Table 1**). In addition, FT-IR was conducted to confirm the biomineralization progress (**Fig. 6**).

After sintering for 30 min, the XRD patterns of BG/water was very similar to those of BG/dry and a green body of BGNs (not shown in Fig. 6). All these showed essentially broad hallo patterns around $2\theta = 15$ to 35°. On the other hand, the changes in XRD peak intensity were observed in BG/SBF for the broad peak at $2\theta = 25$ to 30°, which related to calcium phosphate phase.[27] Especially, BG/SBF was still amorphous whereas the conventionally sintered BGNs had crystalline hydroxyapatite phase after sintering at 850 °C. Based on the results of Vickers hardness test and XRD observation, it should be noted that the BG/SBF having amorphous phase showed better Vickers hardness value even though BG/850 contained the crystalline phase associated with hydroxyapatite.

As mentioned above, the XRD intensity changes of BG/SBF were affected by a formation of amorphous calcium phosphate by the biomineralization, and this agreed with the XRF results. In the case of BG/water, SiO_2 decreased by 0.95 mol %, and CaO and P_2O_5 slightly increased in comparison with BG/dry (Table 1). This compositional change resulted from the precipitation of the ions, released from the dissolved BGNs by distilled water only. On the other hand, the composition of BG/SBF showed 4 mol % lower SiO_2, 3 mol % higher CaO, and 0.6 mol % higher P_2O_5 than that of BG/dry, respectively. This compositional change is related to the formation of the calcium phosphate phase by the precipitation of Ca^{2+} and phosphate ions from SBF solution and partial dissolution of BGNs.

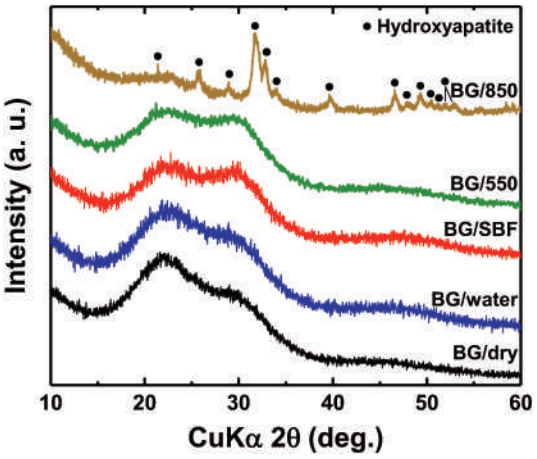

Fig. 5. XRD patterns of BGNs sintered for 30 min under dry, water, and SBF conditions, and the conventionally sintered BGNs (JCPDS: 09-0432).

As shown in Fig. 6, FT-IR spectra of the sintered samples showed different absorption peaks depending on the biomineralization. In BG/SBF and BG/water, two O–H peaks were observed at 1636 and 3446 cm^{-1} [Fig. 6(a)]. These peaks correspond to silanol, resulting from disconnection of the silicate networks by the aqueous solutions such as SBF solution and the distilled water.[28] As shown in Fig. 6(b), the highest peak at 1100 cm^{-1} was attributed to Si–O–Si bonds from BGNs in all the samples.[29] However, in BG/SBF and BG/water, the peaks at 568 and 1189 cm^{-1}, which represent the phosphate groups, were observed.[30] In addition, BG/SBF showed another P–O peak at 601 cm^{-1} that related to the calcium phosphate phase. These observations demonstrated that the amorphous calcium phosphate phase was formed in BG/SBF by biomineralization during LMSP. Therefore, it is concluded that the densification of BGNs is affected by the biomineralization.

Table 1. Compositional changes of the sintered BGNs analyzed by XRF (mol %)

Samples	SiO_2	CaO	P_2O_5	Impurity
BG/dry	56.27	40.95	2.76	0.02
BG/water	55.32	41.67	2.90	0.11
BG/SBF	52.57	44.01	3.34	0.08

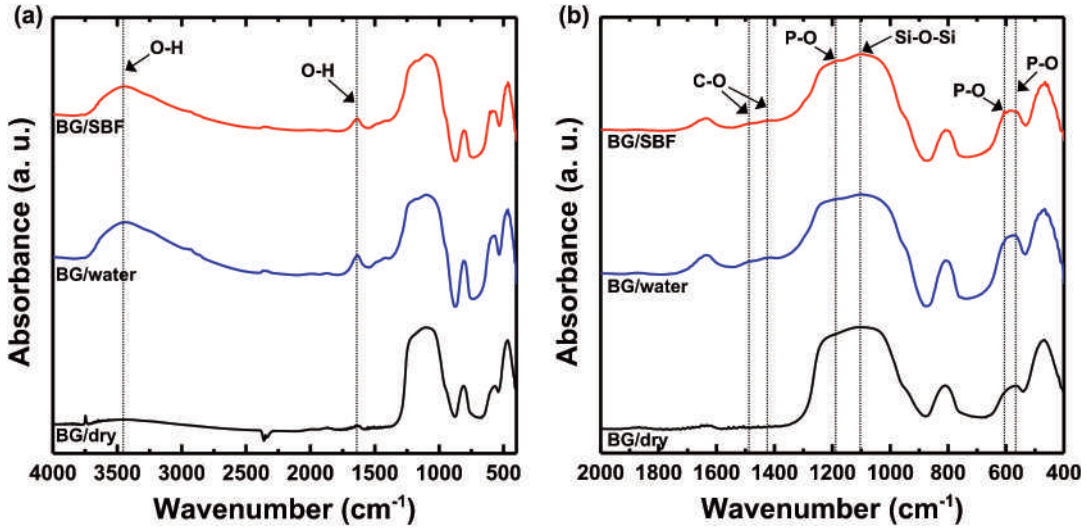

Fig. 6. Full range (a) and magnified (b) FT-IR spectra of the sintered BGNs prepared without using any solution (BG/dry), with pure water (BG/water), and with SBF solution (BG/SBF) conditions.

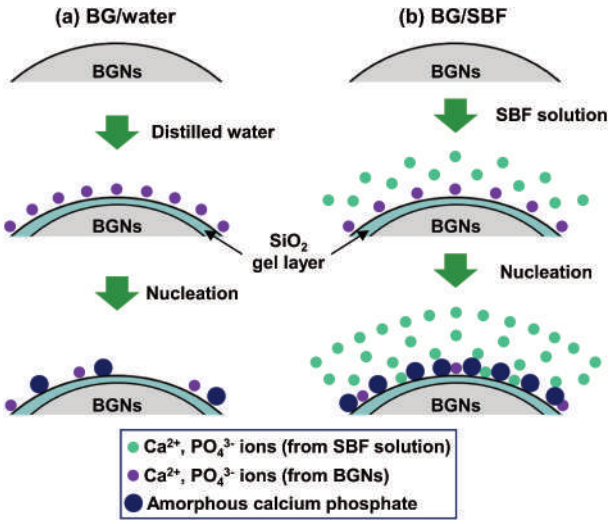

Fig. 7. Schematic drawing of difference of precipitation behavior between (a) BG/water and (b) BG/SBF.

3.4 Effect of supersaturation on biomineralization for densification

The densification in LMSP is based on the biomineralization by which amorphous calcium phosphate was formed at particle–particle interfaces. The aqueous solution significantly influences the nucleation of amorphous calcium phosphate because the growth of amorphous calcium phosphate is different, depending on supersaturation. The velocity of nucleus growth (V) is given by the Nernst-Noyes equation:[31)]

$$V = \frac{D}{S} \cdot O \cdot P \qquad (1)$$

where D is the diffusion coefficient, S is the thickness of the adherent film, O is the extent of surface, and P is the absolute supersaturation. According to the above equation, the velocity of nucleus growth is directly proportional to the absolute supersaturation.

As shown in **Fig. 7**(a), in the case of BG/water, the distilled water dissolves BGNs that released Ca^{2+} and PO_4^{3-} ions in the present case. Then, the only released ions are precipitated from the liquid phase in a BGNs compact under uniaxial pressure and heat. At this point, when the high fraction of the ions is used up for the nucleation of the calcium phosphate, the velocity of nucleus growth is strikingly restricted[32)] due to the lower concentration of chemical species (hence ion activity) that is far from supersaturation state around the surfaces of BGNs in nanoscale fluid, resulting in low relative density of the sintered BGNs such as BG/water. Due to this insufficient formation of calcium phosphate in BG/water, the interfaces between BGNPs could be mainly composed of an amorphous SiO_2 gel layer that was resulted from the dissolution of BGNs by the distilled water. Therefore, BG/water would be fractured in the SiO_2 gel layer, in other words cracks propagate through this layer during the Vickers indentation test.

On the other hand, in the case of BG/SBF [Fig. 7(b)], the bioactive glass networks are partially disconnected by H_3O^+ ions from SBF solution, and Ca^{2+} and PO_4^{3-} from the glass networks are eluted. Then, Ca^{2+} and PO_4^{3-} ions, which migrate not only from the glass networks but also from the SBF solution, are precipitated at the surfaces of BGNs because the SBF solution is supersaturated with respect to apatite.[33)] Finally, the precipitate becomes as the amorphous calcium phosphate, but this formation highly densifies BGNs by filling the pores and vacant areas through the biomineralization. In this case, the amounts of the Ca^{2+} and PO_4^{3-} ions from the SBF solution are greater than those from the glass networks.

Additionally, the supersaturation degree of the liquid phase at the particles boundaries might be further increased by evaporation of water from the SBF solution through the space between the mold punch and die upon heating at 120 °C during the process. Therefore, after the nucleation, there are still enough amount of Ca^{2+} and PO_4^{3-} ions to accelerate the growth of the amorphous calcium phosphate, which agrees with the above Eq. (1). Moreover, sufficient formation of amorphous calcium phosphate in the BG/SBF sample has a beneficial effect on increasing its Vickers hardness value (2.09 GPa), which was higher than that of BG/water saple (1.52 GPa) as mentioned before. Thus, biomineralization by SBF solution is more effective and useful to obtain the sintered BGNs with higher density.

4. Conclusion

Bioactive glass nanoparticles with 30 nm in diameter were prepared by the sol–gel method. Then, the BGNs were successfully densified by biomineralization using SBF solution with 86 % of theoretical density. The processing temperature for densification was just 120 °C enough to evaporate water component of the solution and the sintering time was 30 min, much shorter than that of conventional sintering process. The applied pressure increased the green body density of BGNs and helped the diffusion of the dissolved ions by the solution. In particular, the supersaturated aqueous solution such as SBF solution was more effective to obtain the dense sintered BGNs because the high concentration gradient of Ca^{2+} and PO_4^{3-} ions of SBF solution promotes the growth of amorphous calcium phosphate phase between BGNs. As a result, it is surprising that the BG/SBF showed higher relative density (~86 %) and Vickers hardness (2.09 GPa) in comparison with the other sintered samples such as BG/dry and BG/water, especially better than the conventionally sintered sample at 850 °C (81 %, 2.02 GPa) which coexisting crystalline HAp phase. In terms of the densification mechanism, this sintering protocol is different from the conventional sintering process. No shrinkages (except for vertical shrinkage driven by the applied uniaxial pressure) and viscous flows were observed because BGNs were densified by growth of the newly formed phase at their interfaces during biomineralization in LMSP. Moreover, even though the high pressure was used in LMSP, the sintering density and mechanical properties of BG/SBF, sintered at 120 °C, were better than

those of BG/550 and BG/850. From these results, we could identify the mechanism of low-temperature sintering process using biomineralization and this can be utilized for the low-cost and energy-saving densification process of ceramic and glass materials.

Acknowledgments This work was supported by the "Dynamic Alliance for Open Innovation Bridging Human, Environment and Materials" in "Network Joint Research Center for Materials and Devices" (MEXT, Japan). XRF and FT-IR analysis observation were performed at the Comprehensive Analysis Center, ISIR, Osaka University, Japan. The authors are grateful to Prof. T. Kozawa and Prof. M. Naito (Joining and Welding Research Institute (JWRI), Osaka University, Japan) for their support of the density measurement by the electronic densimeter.

References

1) M. N. Rahaman, Sintering of Ceramics. CRC Press, Boca Raton, Florida (2007).
2) X. Kuang, G. Carotenuto and L. Nicolais, *Adv. Perform. Mater.*, 4, 257–274 (1997).
3) I.-W. Chen and X.-H. Wang, *Nature*, 404, 168–171 (2000).
4) R. M. German, P. Suri and S. J. Park, *J. Mater. Sci.*, 44, 1–39 (2009).
5) I. Tanaka, G. Pezzotti, T. Okamoto and Y. Miyamoto, *J. Am. Ceram. Soc.*, 72, 1656–1660 (1989).
6) O. Guillon, J. Gonzalez-Julian, B. Dargatz, T. Kessel, G. Schierning, J. Räthel and M. Herrmann, *Adv. Eng. Mater.*, 16, 830–849 (2014).
7) R. Z. LeGeros, *Chem. Rev.*, 108, 4742–4753 (2008).
8) F. Barrère, C. A. van Blitterswijk and K. de Groot, *Int. J. Nanomed.*, 1, 317–332 (2006).
9) D. Eglin, S. Maalheem, J. Livage and T. Coradin, *J. Mater. Sci. Mater. Med.*, 17, 161–167 (2006).
10) J. R. Jones, *Acta Biomater.*, 9, 4457–4486 (2013).
11) J. M. Gomez-Vega, E. Saiz, A. P. Tomsia, G. W. Marshall and S. J. Marshall, *Biomaterials*, 21, 105–111 (2000).
12) E. Verné, C. F. Vallés, C. V. Brovarone, S. Spriano and C. Moisescu, *J. Eur. Ceram. Soc.*, 24, 2699–2705 (2004).
13) L. L. Hench, *J. Am. Ceram. Soc.*, 81, 1705–1728 (1998).
14) J. Guo, H. Guo, A. Baker, M. T. Lanagan, E. R. Kupp, G. L. Messing and C. A. Randall, *Angew. Chem. Int. Edit.*, 55, 11457–11461 (2016).
15) J. P. Maria, X. Kang, R. D. Floyd, E. C. Dickey, H. Guo, J. Guo, A. Baker, S. Funihashi and C. A. Randall, *J. Mater. Res.*, 31, 3205–3218 (2017).
16) H. Guo, A. Baker, J. Guo and C. A. Randall, *J. Am. Ceram. Soc.*, 99, 3489–3507 (2016).
17) S. Funahashi, E. Kobayashi, M. Kimura, K. Shiratsuyu and C. A. Randall, *J. Ceram. Soc. Jpn.*, 127, 899–904 (2019).
18) H. Guo, A. Baker, J. Guo and C. A. Randall, *ACS Nano*, 10, 10606–10614 (2016).
19) F. Bouville and A. R. Studard, *Nat. Commun.*, 8, 14655 (2017).
20) S. S. Berbano, J. Guo, H. Guo, M. T. Lanagan and C. A. Randall, *J. Am. Ceram. Soc.*, 100, 2123–2135 (2017).
21) T. Kokubo and H. Takadama, *Biomaterials*, 27, 2907–2915 (2006).
22) Z. Hong, R. L. Reis and J. F. Mano, *J. Biomed. Mater. Res. A*, 88A, 304–313 (2009).
23) T. Kokubo, H. Kushitani, S. Sakka, T. Kitsugi and T. Yamamuro, *J. Biomed. Mater. Res.*, 24, 721–734 (1990).
24) R. Mathew, C. Turdean-Ionescu, B. Stevensson, I. Izquierdo-Barba, A. García, D. Arcos, M. Vallet-Regí and M. Edén, *Chem. Mater.*, 25, 1877–1885 (2013).
25) S. Inaba and S. Fujino, *J. Am. Ceram. Soc.*, 93, 217–220 (2010).
26) C. Ohtsuki, T. Kokubo and T. Yamamuro, *J. Non-Cryst. Solids*, 143, 84–92 (1992).
27) A. C. Tas, *J. Mater. Chem. B*, 1, 4511–4520 (2013).
28) S. M. Ahmadi, A. Behnamghader and A. Asefnejaad, *Dig. J. Nanomater. Bios.*, 12, 847–860 (2017).
29) J. Román, S. Padilla and M. Vallet-Regí, *Chem. Mater.*, 15, 798–806 (2003).
30) H. Takadama, H.-M. Kim, T. Kokubo and T. Nakamura, *Chem. Mater.*, 13, 1108–1113 (2001).
31) H. B. Weiser and W. O. Milligan, *J. Phys. Chem.*, 36, 1950–1959 (1932).
32) W. Chen, T. Long, Y.-J. Guo, Z.-A. Zhu and Y.-P. Guo, *RSC Adv.*, 4, 185–191 (2014).
33) L. Müller and F. A. Müller, *Acta Biomater.*, 2, 181–189 (2006).